ON THE EFFECT OF INJECTION PRESSURE ON SPRAY COMBUSTION AND SOOT FORMATION PROCESSES OF GASOLINE/SECOND GENERATION BIODIESEL BLEND

by

Nasreldin M. MAHMOUD[a, b*], Wenjun ZHONG[b], Qian WANG[b*], Qifei YUAN[b], and Zhixia HE[b]

[a] Mechanical Engineering Department, Faculty of Engineering, University of Sinnar, Sinnar, Sudan
[b] School of Energy and Power Engineering, Jiangsu University, Zhenjiang, China

Original scientific paper
https://doi.org/10.2298/TSCI240109156M

The 70 GB, which comprises 70% gasoline and 30% biodiesel, shows excellent potential for application in gasoline compression ignition due to its superior lubrication capability, renewability, environmental friendliness, high ignitability contributed by biodiesel namely as hydrogenated catalytic biodiesel (HCB), and high volatility conferred by gasoline. However, the spray combustion and emission characteristics of 70 GB fuel have not yet been quantitatively evaluated. In this work, we performed a comprehensive simulation focusing on the ignition delay, heat release rate, flame lift-off length, flame structure, and soot formation of 70 GB in a constant volume chamber under various fuel injection pressure. Numerical results showed that, different injection pressure strongly impact the heat release rate without affecting the maximum temperature. Increasing the injection pressure from 80-120 MPa, increased the heat release rates by 23%. The ignition delay was marginally affected by increasing injection pressure, while a 5.7 mm increase in flame lift-off length observed with higher injection pressure. Additionally, 65% lower soot formation was typically predicted for higher injection pressure 120 MPa. In particular, the soot mass is primarily controlled by enhancing the atomization and evaporation processes, as well as improving fuel-air mixing rate, which was achieved by increasing the injection pressure. Furthermore, the role of soot oxidation was insignificant in reducing soot with increasing injection pressure, while the soot initiation step and soot surface growth step play an important role in soot suppression with increasing injection pressure for 70 GB fuel.

Key words: *gasoline-HCB blends, CFD simulation, operation conditions, flame structure, soot formation*

Introduction

Low temperature combustion (LTC) mode become increasingly popular in the transportation sector that aimed at achieving high thermal efficiency while reducing emissions [1-4]. The LTC can be achieved by diverse strategies including homogeneous charge compression ignition (HCCI), premixed charge compression ignition (PCCI), reactivity controlled compression ignition (RCCI), and gasoline compression igniting (GCI) [1, 2]. Compared with different LTC strategies, GCI has the advantage of higher octane number and volatility due to gasoline fuel, thus improving fuel-air pre-ignition, enhancing combustion performance, and

* Corresponding authors, e-mail: nasrmohamed53@hotmail.com; qwang@ujs.edu.cn

reducing emissions [5-7]. However, these advantages can also lead to ignition difficulties especially under low loads, as well as high pressure rise rates at high loads [8]. In addition, due to the low viscosity of gasoline, fuel injection systems (FIS) can be easily damaged at high injection pressures [9]. Therefore, researchers are making efforts to improve the GCI mode through fuel design [10].

In contrast to gasoline, fuel with high ignitability, such as diesel [1] or biodiesel [11, 12], offers the potential to enhance the overall reactivity and solve the ignition difficulties of GCI engines, especially under low load. The HCB is particularly attractive as a renewable biodiesel fuel that can be derived from waste cooking oil via one-step hydrogenation [13]. In contrast to most first-generation biodiesels, it is not expected to compete with food supplies. The HCB fuel has a straight-chain molecular structure and is composed of large carbon molecular chains (C_{14}-C_{16}) [14, 15]. It is characterized by the absence of aromatics, low volatility, oxygen-free content, low fuel density, and superior lubricating capability [13, 16, 17]. The high reactivity of HCB can alleviate the ignition difficulties of GCI [15-19]. Furthermore, HCB has superior lubricity and therefore, has high potential for solving the problem of low lubrication in GCI engines [20, 21]. Thus, HCB-gasoline blends are believed to be a promising fuel for GCI engines and have been previously studied in existing GCI engines [15-19]. The spray, ignition, and combustion properties of pure HCB and two different gasoline-HCB blends (gasoline with 30% HCB and 50% HCB) have been studied in a CVCC under GCI engine-relevant conditions [16]. Interestingly, with the increase in the HCB ratio from 30-50% in the blend, the ignition delay and lift-off length decreased by 31.8% and 18%, respectively, whereas spray liquid length showed the opposite trend (23.9% increase) at ambient temperature of 900 K. Zhang *et al.* [17] investigated the effect of gasoline with three addition ratio of HCB (20%, 30%, and 40%) on the combustion characteristics of a heavy-duty diesel engine. They reported notable improvements in ignition characteristics with the increase in HCB ratio. In particular, increasing HCB ratio from 20-40% suppressed the maximum combustion pressure by about 3.4%. Another research investigated the effect of gasoline-HCB fuel on the combustion and emissions of GCI engines through single and multiple injection approaches [19]. The research concluded that the multiple injection mode could notably reduce the pressure rise rate and PM of gasoline-HCB blends by about 31% and 37%, respectively. However, pollutants, such as CO and UHC, were slightly increased in multiple injection mode relative to the single injection mode. Overall, gasoline-HCB blends are a promising form of fuel for alleviating GCI engine limitations and improving engine combustion and emission. However, previous works have shown that soot in flame was slightly increased due to the increased of precursor species (*i.e.* acetylene) [22-24].

Another strategy for improving the fuel-air mixing and controlling soot in flame, which is fuel injection pressure. Previous study reported that higher injection pressure is more conducive to improve fuel air mixing and combustion efficiency [25-30]. Wang *et al.* [25, 31, 32] studied the effect of injection pressure on biodiesel and diesel combustion and emissions, and their experimental results showed that increasing injection pressure was beneficial to decrease soot emissions. Kuti *et al.* [33] investigated the combustion performance of palm oil biodiesel with three different injection pressures 100 MPa, 200 MPa, and 300 MPa, and they concluded that the ignition delay decreased by about 27.2% with increasing the injection pressure from 100-300 MPa and the combustion process was effectively improved. Yu *et al.* [34] studied the spray characteristics of diesel fuel at a high injection pressure using large eddy simulation, and their results showed that high injection pressure could significantly improve the atomization effect. However, different results were observed by Shi *et al.* [35] where they found that the heat release rate (HRR) is affected by the high injection pressure due to the

decreasing mixture fraction that below the stoichiometric mixture fraction (Z^{st}). In our previous study [30] we investigated the spray and evaporation characteristics of a binary fuel composed of 20% *n*-pentanol and 80% *n*-dodecane fuel under various injection pressure ranged from 100-300 MPa. The results concluded that the application of extremely elevated injection pressure significantly enhanced the spray penetration by about 20%, while concurrently diminishing the size of droplets. This, in turn, resulted in the fragmentation of fuel droplets and effectively enhanced the overall atomization characteristics. From aforementioned review, it is clear that most previous studies of gasoline-HCB blends focused only on the combustion and emission characteristics in engines, and fundamental numerical studies on the combustion and emission characteristics of gasoline-HCB blends are rare. Therefore, a simulation investigation was conducted on 70 GB by varying the injection pressure in a constant volume combustion chamber to explore its effects on the spray combustion and emissions. The injection pressure was varied within the range of 80-120 MPa.

Model and numerical set-up

Model descriptions

In this study, 3-D simulations were performed with the CONVERGE package [36]. The details of the combustion chamber and the numerical models have been discussed in a previous studies [22, 37]. In brief, the numerical model solves the fully coupled elliptic conservation equations. The finite volume method is used to discretize the governing equations. A modified pressure implicit with splitting of operator (PISO) method [38] to handle the pressure and velocity coupling and to solve the discretized equations. The convective term is discretized using a flux scheme. Turbulence was modelled using the RNG *k-e* turbulence model [20]. The spray breakup process has been described by the Kelvin-Helmholtz (KH) and Rayleigh-Taylor (RT) model without a breakup length [39]. The droplet collisions was described by the no-time counter (NTC) algorithm proposed by Schmidt and Rutland [40]. The droplet evaporation process was described based on the Froessling correlation method [41]. The governing equations solved with point-wise successive over-relaxation (SOR) algorithm with a relaxation factor for accelerating convergence. A variable time-step is used for calculation with minimum and maximum time step size is $1 \cdot 10^{-7}$ and $1 \cdot 10^{-5}$ [second]. The computations were performed on a 3-D cylindrical domain of 100 mm × 120 mm to simulate the constant volume combustion chamber as previous work as presented in fig. 1. For all cases, the base grid size was fixed at 4 mm as -cited in many previous studies [22, 37, 42]. To resolve the flow near the injector, three scales of fixed embedding are employed to refine the grid at the flow near the injector such that the minimum grid size is 0.5 mm based on a previous study [22, 37]. It is rather difficult to determine a priori where a refined grid is needed. Hence, different levels of adaptive mesh refinement (AMR) for the mesh sensitivity test. In particular, different levels of AMR scales are

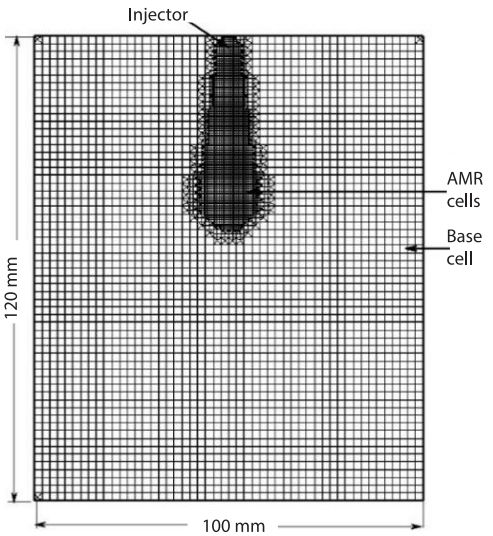

Figure 1. Shows the Cartesian grid created in CONVERGE package at 1 ms after start of injection (ASOI)

employed for the velocity field namely 2, 3, and 4 levels of AMR scales, which are corresponding to the minimum grid sizes of 1 mm, 0.5 mm, and 0.25 mm, respectively. Although not shown, the spray penetration was well predicted by the different AMR scales. In addition, reasonable grid convergence could be achieved with a minimum grid size of 0.5 mm and 0.25 mm. However, to achieve the accuracy of the results with minimum computational cost, AMR with three levels was adopted wish is corresponding to minimum grid size of 0.5 mm. The convergence criteria was set to be $1 \cdot 10^{-5}$ for the momentum equation, while for the energy, density, and species equations it was $1 \cdot 10^{-7}$.

To model the combustion process, the SAGE detailed chemical kinetic solver was used [43] coupled with the gas-phase calculations in CHEMKIN-formatted input files. To accelerate the solution process, the multi-zone model solves the SAGE detailed chemical kinetics in zones. n-hexadecane (n-$C_{16}H_{34}$) was chosen here as surrogate for HCB fuel, due to the similar cetane number (~100) and its relative abundance in the HCB composition [14, 22].

Kinetic mechanism and soot model

The combined reduced mechanism of n-hexadecane/TRF developed in our previous study was employed in the present simulation [22]. The combined reduced mechanism consist of 116 species and 495 chemical reactions. This mechanism was combined from the mechanism of toluene reference fuel (TRF) consisting of 109 species and 543 reactions which was developed by Wang *et al.* [44] and the skeletal mechanism of heavy *n*-Alkanes consisting of 80 species and 194 reactions which was developed by Chang *et al.* [45]. Additional reactions to form benzene (A1) and describe the growth kinetics of larger PAH were taken from the mechanism of Pang *et al.* [46]. The final reduced mechanism involves 116 species and 495 reactions. The soot formation was simulated by the practical phenomenological soot model [47-49] accounts for soot inception, surface growth through C_2H_2 assisted, coagulation, and oxidation by OH and O_2. More details about kinetic mechanism and soot model can be found elsewhere [22].

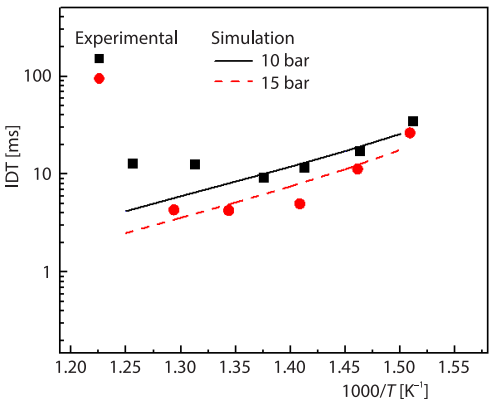

Figure 2. Comparison between simulated IDT and experimental data measured in [50] of 70 GB at $\phi = 1$ and two different pressure of 10 bar and 15 bar

Mechanism and model validations

Before presenting a detailed analysis of the various parameters effect, we first validate the *n*-hexadecane/TRF mechanism with a heated rapid compression machine (RCM) experiments reported our previous work [50]. Figure 2 shows the comparison of the predicted ignition delay time with measured ignition delay timings of 70 GB/air mixture. The simulations were performed with the Closed Homogeneous Reactor module within ANSYS Chemkin software [51], at two different pressures of 10 bar and 15 bar, and equivalence ratio of 1. As shown in fig. 2, the computed ignition delay times by using the current mechanism showed satisfactory agreements with the experimental data, although the simulation slightly under-estimates the ignition delay times at $T > 750$ K with a maximum difference of about a factor of 3 at pressure of 10 bar. Overall, the present mechanism captures the change of ignition delay times with different two pressures.

We next validate the spray model by comparing the experimental and predicted results under evaporating sprays of 70 GB fuel. Figure 3 shows the comparison of previous experimental [18] and current computed temporal evolution of liquid spray penetration profiles of 70 GB fuel. It is clear seen that the simulation under-predicts the spray penetration at the early stage of injection <1000 μs after start of injection (ASOI) but agrees well with the experimental data at later times. The maximum error for the predicted spray penetration is about 30.1% at early stage of injection (100 μs), while at time >1000 μs ASOI the maximum error is 4.6%.

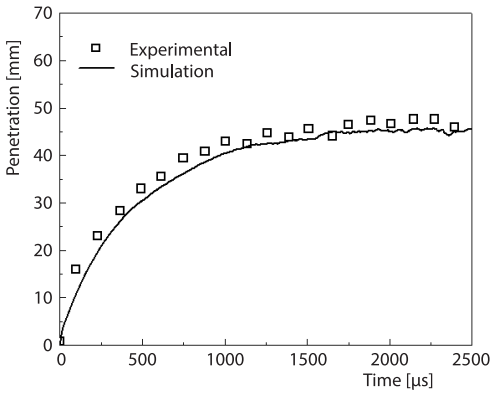

Figure 3. Comparisons between experimental and simulated liquid spray penetration for 70 GB

Experimental and simulations for comparison of the liquid phase development result of evaporating sprays are shown in fig. 4. Although the model under estimate the measurement slightly at earlier time of injection, the overall simulation well captures the structure/development observed in the experiment [18] for 70 GB fuel.

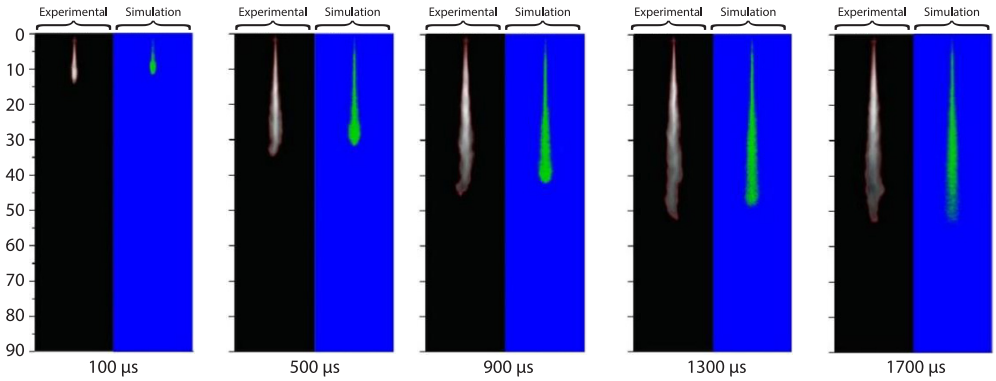

Figure 4. Comparison between experimental and simulated liquid phase development under evaporating sprays at different times for 70 GB

Results and discussions

Effect of injection pressure on combustion characteristics

Previous study reported that higher injection pressure is more conducive to improve fuel air mixing and combustion efficiency [25-27]. However, different results were observed by Shi *et al.* [35] where they found that the HRR was affected by the high injection pressure due to the decreasing mixture fraction that below the Z^{st}. Thus, three different injection pressure of 80 MPa, 100 MPa, and 120 MPa were investigated in this study. Here, the initial ambient temperature and ambient oxygen concentration were fixed at 900 K and 15%, respectively. Figure 5 shows the maximum temperature and heat release rate for 70 GB under three different injection pressures. It can be seen from the figure, the increase of injection pressure slightly decrease the ignition delay (second ignition delay). Furthermore, the increase of injection pressure of the 70 GB blend leads to an increase in heat release rate with no significant differences in maxi-

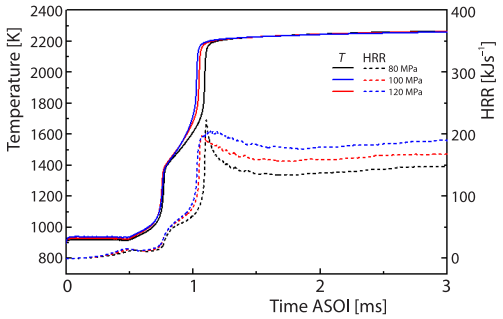

Figure 5. Combustion temperature and HRR for 70 GB under different injection pressures

mum flame temperatures. This computed result is in line with the results concluded by several authors in the literature with different fuels [25-27, 35], in which, higher injection pressure leads to finer break-up, smaller droplets, quicker evaporation, and more intense air entrainment, finally resulting in a quicker formation of ignitable mixture [52]. At first glance, this may seem to be different from the observation of Shi *et al.* [39], in which the HRR was seen to be affected negatively with increasing injection pressure. As a matter of fact, this difference is mainly due to the different in ambient conditions. In details, previous studies [25-27, 35] were conducted at a relatively high temperature ambient. In this case, the combustion is controlled by the fuel mixing and air entrainment, and the spray combustion belongs to mixing controlled diffusion flame concept [53]. On the other hand, the study of Shi *et al.* [35] was conducted at a cold start conditions. In the case of cold start condition, the spray is similar to the concept of partially premixed low temperature combustion [54]. Thus, the heat release decreases with higher injection pressure in the work of Shi *et al.* [35] due to transfer the spray combustion regime from non-premixed combustion lean-premixed combustion (mixture fraction below the Z^{st}).

The influence of injection pressure on igniting delay time (ID) and flame lift-off length (FLOL) with three different injection pressures was presented in fig. 6(a). Here, the ID is define as the time taken for the mixture to increase by 400 K from its initial temperature, while FLOL is defined as the upstream distance to which the OH mass fraction reach 2% of its maximum. As can be seen from fig. 6, the computed ID affected negligibly with increasing injection pressure. However, FLOL demonstrate 12.8% increase as injection pressure increase from 80-120 MPa. This result is in line with finding of [33]. The increase of FLOL with increasing injection pressure may be attributed to the higher spray velocities which arise at higher injection pressures, which is confirmed in fig. 6(b). It can be observed from the figure that, as injection pressure increased from 80 MPa to value of 120 MPa, the peak spray velocity increased by 24.4%. This

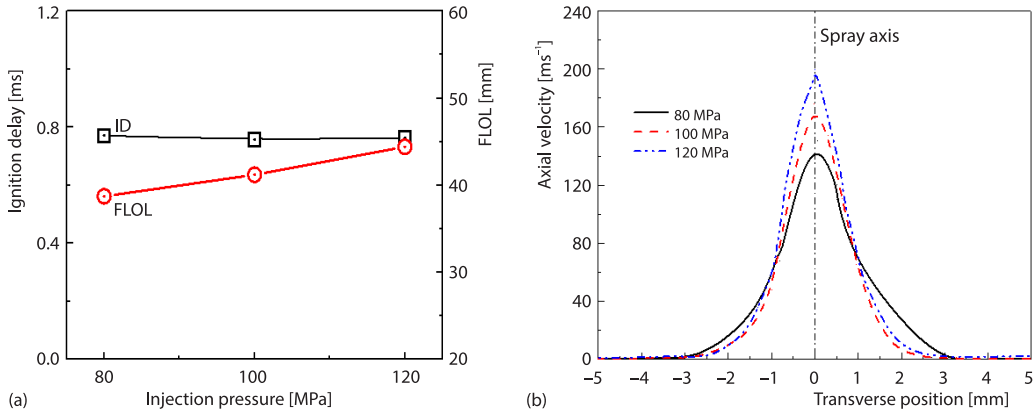

Figure 6. Predicted (a) ID (black line) and FLOL (red line) and (b) axial velocity 15 mm away from injector nozzle at 2 ms ASOI with three different injection pressure

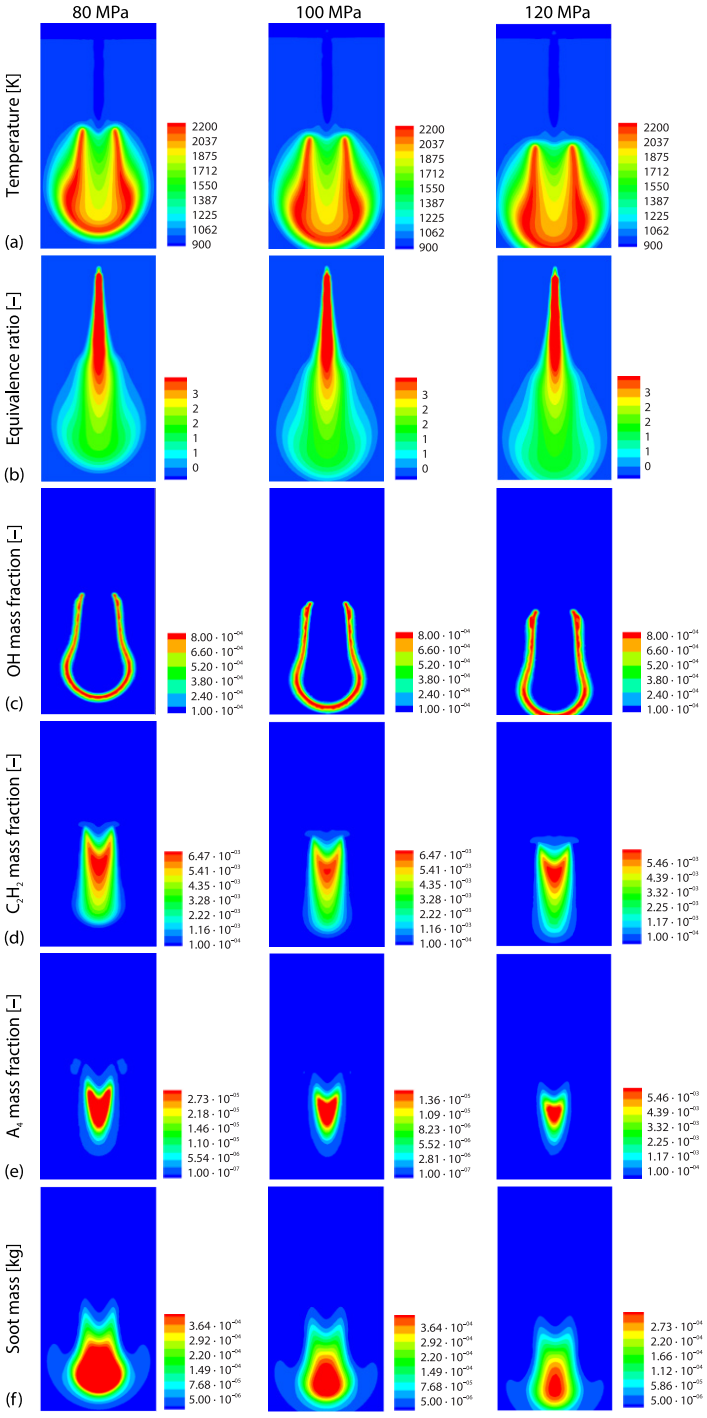

Figure 7. The mass fraction contours of temperature, equivalence ration, OH, C_2H_2, A4, and soot mass for 70 GB under three different injection pressures of 80 MPa, 100 Mpa, and 120 MPa

increased in spray velocity pushing the initial combustion zone further downstream, which reveal the longer FLOL with higher injection pressure.

Effect of injection pressure on flame structure and soot formation

Figure 7 shows the computed contours of temperature, equivalence ratio, and mass fraction of OH, C_2H_2, and A4 along with soot mass for 70 GB under three different injection pressures of 80 MPa, 100 MPa, and 120 MPa. As can be seen from fig. 7(a), with the increase of fuel injection pressure, the high temperature zone becomes relatively larger. Furthermore, the flame shifted further downstream when the pressure is increased. As presented in fig. 7(c), the maximum OH mass fraction increases by 20% when the pressure increases from 80-120 MPa. This implies that an increase in injection pressure generate more fine droplets, thereby increasing the entrained oxidizer and producing more OH substances. Moreover, the OH distribution consist with that of temperature, which is located further downstream for higher injection pressure as shown in fig. 7(b). Again, the contour of OH mass fraction confirm that, the FLOL increases with the increase in injection pressure. It is known that the local mixing and turbulence conditions play an important role on the distance of FLOL [22]. As the injection pressure increases, the increase in velocity causes the mixture to move downstream before ignition as discussed earlier. The formation of the C_2H_2 and A4 diminished by 14.8% and 61.6% with the increase of the injection pressure from 80-100 Mpa, and the formation area becomes relatively smaller and extended further downstream. Soot mass also decreases by about 65% when the pressure increases from 80-120 MPa being consist with C_2H_2 and A4 distribution. The main reasons may be due to improved atomization, evaporation and faster fuel-air mixing rate at 120 MPa. Although not shown, the sauter mean diameter (SMD) decreased as injection pressure increased, which is similar to previous stuied [55, 56]. The decrease in SMD with injection pressure will enhance the entrainment of air into the spray [30]. The enhancement in

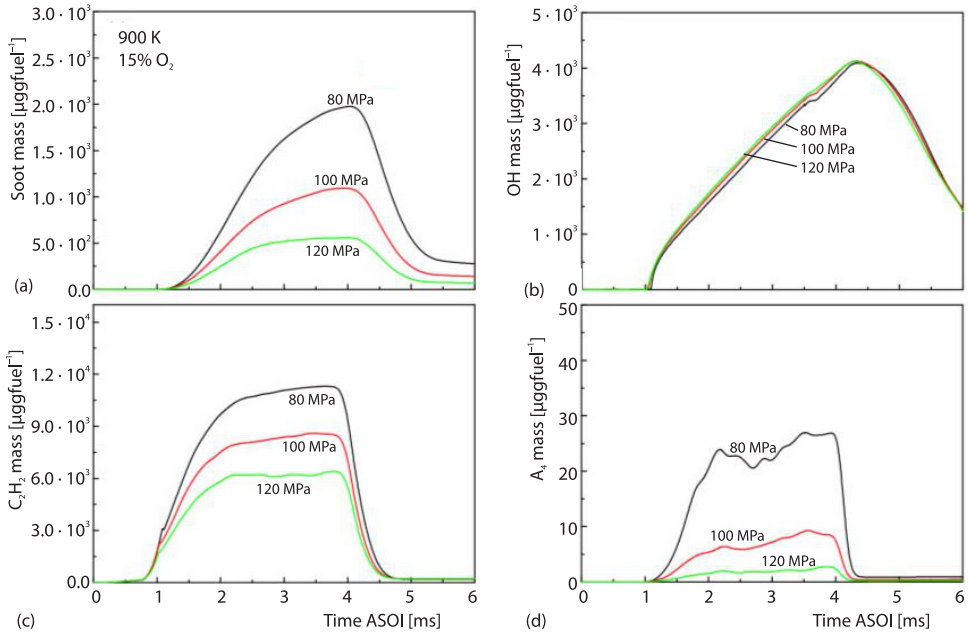

Figure 8. The computed profile of (a) soot mass, (b) OH, (c) C_2H_2, and (d) A4 for the three different injection pressure

the quantity of air entrained has greater tendency of promoting vaporization of the spray, which was beneficial to inhibit the formations of precursors and soot.

The computed profiles of soot mass and OH radical, acetylene (C_2H_2) and pyrene (A4) were also further illustrated in fig. 8. The computaions were performed under initial ambient temperature of 900 K with ambient oxygen concentration of 15%. As illustrateed in fig. 8(a), as the injection pressure of 70 GB increases, the profile of soot significantly decreases. This is largely due to the fact that, the profile of soot prescurser species (C_2H_2 and A4) decreases with the increase of injection pressure, as shown in figs. 8(c) and 8(d), respectively, which is beneficial for suppressing the intiation and furture growth rate of soot. Furthermore, it is evident that, the initiation of soot profile is retarded with higher injection pressure of 120 MPa, which corresponds to its longer FLOL. It is well known that, OH radical is reactive oxidizing agent, that can greatly promote the oxidation of soot and other intermediate substances during the reaction process. As shown in fig. 8(b), as the injection pressure increases, the formation of OH radicals is negligible affected. Consequently, OH oxidation does not play a role in reducing soot as the injection pressure increases. On the contrary, as the injection pressure increases, the distribution of C_2H_2 and A4 shows a decrease. This suggests that the soot inception step and soot surface growth step plays a significant role on soot supresstion with increasing injection pressure for 70 GB fuel.

Conclusion

A CFD simulation study was performed to investigate the effects of fuel injection pressure on spray characteristics, flame structure, and soot process of 70 GB. The computations were performed in a constant volume combustion chamber under initial ambient temperature of 900 K, ambient oxygen concentration of 15%, and three different injection pressures of 80 MPa, 100 MPa, and 120 MPa. The numerical results concluded that, with the increase of injection pressure, HRR increased monotonically, while the maximum flame temperature remained relatively constant without any noteworthy changes. Moreover, FLOL demonstrated an increase as injection pressure increases, which attributed to increased spraying velocity and improved mixing effect. However, no significant changes were observed in the ignition delay. Numerical results also showed that as the injection pressure increase, OH formation increased slightly, whereas C_2H_2 and A4 formation decreased significantly. According to HACA mechanism, decreased C_2H_2 concentration tends to prevent the surface growth process of soot and larger PAH formation. In addition, decreased A4 concentration tends to inhibit the inception step of soot. Furthermore, the role of increased FLOL associated with increased injection pressure in reducing and retarding soot formation was emphasized.

Acknowledgment

This work is supported by the National Natural Science Foundation of China (No. 52076103). The NMM acknowledges the University of Sinnar for additional financial support.

References

[1] Chaudhari, V. D., Deshmukh, D., Diesel and Diesel-Gasoline Fuelled Premixed Low Temperature Combustion (LTC) Engine Mode for Clean Combustion, *Fuel*, *266* (2020), 116982,
[2] Krishnamoorthi, M., *et al*., A Review on Low Temperature Combustion Engines: Performance, Combustion and Emission Characteristics, *Renewable and Sustainable Energy Reviews*, *116* (2019), 109404
[3] Cracknell, R. F., *et al.*, Modelling a Gasoline Compression Ignition (GCI) Engine Concept, Report, SAE Technical Paper, 2014-01-1305, 2014
[4] Rose, K., *et al*., Exploring a Gasoline Compression Ignition (GCI) Engine Concept, Report, SAE Technical Paper, 2013-01-0911, 2013

[5] Tuner, M., *et al.*, Multi Cylinder Partially Premixed Combustion Performance Using Commercial Light-Duty Engine Hardware, SAE Technical Paper, 2014-10-13, 2014
[6] Zelenyuk, A., *et al*., Detailed Characterization of Particulates Emitted by Pre-Commercial Single-Cylinder Gasoline Compression Ignition Engine, *Combustion and Flame*, *161* (2014), 8, pp. 2151-2164
[7] Hunicz, J., *et al.*, Late Direct Fuel Injection for Reduced Combustion Rates in a Gasoline Controlled Auto-Ignition Engine, *Thermal Science*, *22* (2018), 3, pp. 1299-1309
[8] Wei, H., *et al.*, Experimental Investigation on Knocking Combustion Characteristics of Gasoline Compression Ignition Engine, *Energy*, *143* (2018), Jan., pp. 624-633
[9] Manente, V., *et al*., Effects of Ethanol and Different Type of Gasoline Fuels on Partially Premixed Combustion from Low to High Load, SAE Technical Paper, 2010-04-12, 2010
[10] Sellnau, M., *et al.*, GDCI Multi-Cylinder Engine for High Fuel Efficiency and Low Emissions, *SAE Int. J. Engines*, *8* (2015), 2, pp. 775-790
[11] Putrasari, Y., Lim, O., A Study on Combustion and Emission of GCI Engines Fueled with Gasoline-Biodiesel Blends, *Fuel*, *189* (2017), Feb., pp. 141-154
[12] Thongchai, S., Lim, O., Investigation of the Combustion Characteristics of Gasoline Compression Ignition Engine Fueled with Gasoline-Biodiesel Blends, *Journal of Mechanical Science and Technology*, *32* (2018), 2, pp. 959-967
[13] Zhong, W., *et al*., Experimental Study of Combustion and Emission Characteristics of Diesel Engine with Diesel/Second-Generation Biodiesel Blending Fuels, *Energy Conversion and Management*, *121* (2016), Aug., pp. 241-250
[14] Xuan, T., *et al*., A Study of Soot Quantification in Diesel Flame with Hydrogenated Catalytic Biodiesel in a Constant Volume Combustion Chamber, *Energy*, *145* (2018), Feb., pp. 691-699
[15] Zhang, Y., *et al*., An Investigation on Gasoline Compression Ignition (GCI) Combustion in a Heavy-Duty Diesel Engine Using Gasoline/Hydrogenated Catalytic Biodiesel Blends, *Applied Thermal Engineering*, *160* (2019), 113952
[16] Zhong, W., *et al*., Experimental Study on Spray and Combustion of Gasoline/Hydrogenated Catalytic Biodiesel Blends in a Constant Volume Combustion Chamber Aimed for GCI Engines, *Fuel*, *253* (2019), Oct., pp. 129-138
[17] Zhang, Y., *et al*., Experimental Study of Combustion and Emission Characteristics of Gasoline Compression Ignition (GCI) Engines Fueled by Gasoline-Hydrogenated Catalytic Biodiesel Blends, *Energy*, *187* (2019), 115931
[18] Yuan, W. H., *et al*., Experimental Study on Spray Characteristics of Gasoline/Hydrogenated Catalytic Biodiesel under GCI Conditions, *Journal of Chemistry*, *2020* (2020), 9, 4285460
[19] Zhong, W., *et al*., Combustion and Emission Characteristics of Gasoline/Hydrogenated Catalytic Biodiesel Blends in Gasoline Compression Ignition Engines under Different Loads of Double Injection Strategies, *Applied Energy*, *251* (2019), 113296
[20] Han, Z., Reitz, R. D., Turbulence Modelling of Internal Combustion Engines using RNG κ-ε Models, *Combustion Science and Technology*, *106* (1995), 4-6, pp. 267-295
[21] Torregrosa, A. J., *et al*., Impact of Gasoline and Diesel Blends on Combustion Noise and Pollutant Emissions in Premixed Charge Compression Ignition engines, *Energy*, *137* (2017), Oct., pp. 58-68
[22] Zhong, W., *et al*., Numerical Study of Spray Combustion and Soot Emission of Gasoline-Biodiesel Fuel Under Gasoline Compression Ignition-Relevant Conditions, *Fuel*, *310* (2022), 122293
[23] Mahmoud, N. M., *et al*., Chemical Effects of CO_2 and H_2O Addition on Aromatic Species in Ethanol/Air Diffusion Flame, *Combustion Science and Technology*, *194* (2022), 3, pp. 589-607
[24] Mahmoud, N. M., *et al*., Flame Structure and Soot-Precursor Formation of Coflow n-Heptane Diffusion Flame Burning in O_2/N_2 and O_2/CO_2 Atmosphere, *Journal of Energy Engineering*, *147* (2021), 4, 04021027
[25] Wang, X., *et al*., Effect of Injection Pressure on Flame and Soot Characteristics of the Biodiesel Fuel Spray, *Combustion Science and Technology*, *182* (2010), 10, pp. 1369-1390
[26] Kahila, H., *et al.*, Large-Eddy Simulation on the Influence of Injection Pressure in Reacting Spray A, *Com*bus*tion and Flame*, *191* (2018), May, pp. 142-159
[27] Pei, Y., *et al.*, Modelling n-Dodecane Spray and Combustion with the Transported Probability Density Function Method, *Combustion and Flame*, *162* (2015), 5, pp. 2006-2019
[28] Bruneaux, G., Liquid and Vapor Spray Structure in High-Pressure Common Rail Diesel Injection, *Atomization and Sprays*, *11* (2001), 5, pp. 533-556
[29] Agarwal, A. K., *et al*., Effect of Fuel Injection Pressure on Diesel Particulate Size and Number Distribution in a CRDI Single Cylinder Research Engine, *Fuel*, *107* (2013), May, pp. 84-89

[30] Zhong, W., *et al*., Spray-Evaporation Characteristics of n-Pentanol/n-Dodecane Binary Fuel at Ultra-High Injection Pressure, *Renewable Energy*, *219* (2023), 119505
[31] Wang, X., *et al.*, Effects of Ultra-High Injection Pressure and Micro-Hole Nozzle on Flame Structure and Soot Formation of Impinging Diesel Spray, *Applied Energy*, *88* (2011), 5, pp. 1620-1628
[32] Wang, X., *et al*., Experimental and Analytical Study on Biodiesel and Diesel Spray Characteristics under Ultra-High Injection Pressure, *International Journal of Heat and Fluid-Flow*, *31* (2010), 4, pp. 659-666
[33] Kuti, O. A., *et al*., Characterization of Spray and Combustion Processes of Biodiesel Fuel Injected by Diesel Engine Common Rail System, *Fuel*, *104* (2013), Feb., pp. 838-846
[34] Yu, S., *et al.*, Numerical Research on Micro Diesel Spray Characteristics under Ultra-High Injection Pressure by Large Eddy Simulation (LES), *International Journal of Heat and Fluid-Flow*, *64* (2017), Apr., pp. 129-136
[35] Shi, Z., *et al.*, Numerical study on The Influence of Injection Pressure on the Ignition and Combustion of n-Dodecane Spray at Cold-Start Conditions, *Fuel*, *264* (2020), 116882
[36] Richards, K., *et al*., CONVERGE (v2.3), Madison (WI): Convergent Science, 2016
[37] Mahmoud, N. M., *et al*., Impact of n-Butanol Addition Hydrogenated Catalytic Biodiesel Fueled a Constant Volume Combustion Chamber, A Computational Study, Energy Sources – Part A: *Recovery, Utilization*, *and Environmental Effects*, *45* (2023), 4, pp. 12553-12569
[38] Issa, R., Solution of the Implicitly Discretised Fluid-flow Equations by Operator-Splitting, *Journal of Computational Physics*, *62* (1986), 1, pp. 40-65
[39] Ricart, L. M., *et al*., Comparisons of Diesel Spray Liquid Penetration and Vapor Fuel Distributions with in-Cylinder Optical Measurements, *Journal of Engineering for Gas Turbines and Power-Transactions of the ASME*, *122* (2000), 4, pp. 588-595
[40] Schmidt, D. P., Rutland, C. J., A New Droplet Collision Algorithm, *Journal of Computational Physics*, *164* (2000), 1, pp. 62-80
[41] Froessling, N., Evaporation, Heat Transfer, and Velocity Distribution in 2-D and Rotationally Symmetrical Laminar Boundary-Layer Flow, *Fysiografiska Sallskapets Handlingar*, *51* (1958), 4
[42] Som, S., Longman, D. E., Numerical Study Comparing the Combustion and Emission Characteristics of Biodiesel to Petrodiesel, *Energy and Fuels*, *25* (2011), 4, pp. 1373-1386
[43] Senecal, P. K., *et al*., Multi-Dimensional Modelling of Direct-Injection Diesel Spray Liquid Length and Flame Lift-off Length Using CFD and Parallel Detailed Chemistry, SAE Technical Paper, 2003-03-03, 2003
[44] Wang, H., *et al*., A Reduced Toluene Reference Fuel Chemical Kinetic Mechanism for Combustion and Polycyclic-Aromatic Hydrocarbon Predictions, *Combustion and Flame*, *162* (2015), 6, pp. 2390-2404
[45] Chang, Y., *et al*., Application of a Decoupling Methodology for Development of Skeletal Oxidation Mechanisms for Heavy n-Alkanes from n-Octane to n-Hexadecane, *Energy and Fuels*, *27* (2013), 6, pp. 3467-3479
[46] Pang, B., *et al*., Development of a Phenomenological Soot Model Coupled with a Skeletal PAH Mechanism for Practical Engine Simulation, *Energy and Fuels*, *27* (2013), 3, pp. 1699-1711
[47] Vishwanathan, G., Reitz, R. D., Development of a Practical Soot Modelling Approach and Its Application Low-Temperature Diesel Combustion, *Combustion Science and Technology*, *182* (2010), 8, pp. 1050-1082
[48] Vishwanathan, G., Reitz, R. D., Application of a Semi-Detailed Soot Modelling Approach for Conventional and Low Temperature Diesel Combustion – Part II: Model sensitivity, *Fuel*, *139* (2015), Jan., pp. 771-779
[49] Vishwanathan, G., Reitz, R. D., Application of a Semi-Detailed Soot Modelling Approach for Conventional and Low Temperature Diesel Combustion – Part I: Model performance, *Fuel*, *139* (2015), Jan., pp. 757-770
[50] Zhong, W., *et al.*, Experimental and Modelling Study of the Autoignition Characteristics of Gasoline/Hydrogenated Catalytic Biodiesel Blends over Low-to-Intermediate Temperature, *Fuel*, *313* (2022), 122919
[51] ***, CHEMKIN 15151, ANSYS Reaction Design: San Diego, Reaction Design, 2016
[52] Dec, J. E., Advanced Compression-Ignition Engines – Understanding the in-Cylinder Processes, *Proceedings of the Combustion Institute*, *32* (2009), 2, pp. 2727-2742
[53] Dec, J. E., A Conceptual Model of DL Diesel Combustion Based on Laser-Sheet Imaging, SAE Technical Paper, 1997-02-24, 1997
[54] Musculus, M. P. B., *et al.*, Conceptual Models for Partially Premixed low-Temperature Diesel Combustion, *Progress in Energy and Combustion Science*, *39* (2013), 2, pp. 246-283

[55] Kuti, O. A., *et al*., Spray Combustion Simulation Study of Waste Cooking Oil Biodiesel and Diesel under Direct Injection Diesel Engine Conditions, *Fuel*, 267 (2020), 117240
[56] Kuti, O. A., *et al*., Experimental Studies on Spray and Gas Entrainment Characteristics of Biodiesel Fuel: Implications of Gas Entrained and Fuel Oxygen Content on Soot Formation, *Energy*, *57* (2013), C, pp. 434-442

Paper submitted: January 9, 2024
Paper revised: May 21, 2024
Paper accepted: May 25, 2024